Egyptian Journal of Petroleum (2016) xxx, xxx–xxx

HOSTED BY

ELSEVIER

Egyptian Petroleum Research Institute

Egyptian Journal of Petroleum

www.elsevier.com/locate/egyjp
www.sciencedirect.com

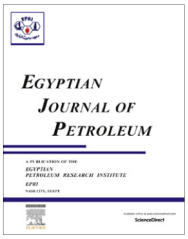

FULL LENGTH ARTICLE

Corrosion inhibition properties of 1,2,4-Hetrocyclic Systems: Electrochemical, theoretical and Monte Carlo simulation studies

Sam John [a,b,*], **Abraham Joseph** [a], **Sajini T.** [b], **Ajith James Jose** [b]

[a] *Department of Chemistry, University of Calicut, 673635 Kerala, India*
[b] *Department of Chemistry, St. Berchmans College Campus, Mahatma Gandhi University Kottayam, 686101 Kerala, India*

Received 17 May 2016; revised 19 August 2016; accepted 16 October 2016

KEYWORDS

Corrosion inhibitor;
Mild steel;
EIS;
DFT;
Fukui;
Monte Carlo simulation

Abstract Inhibition of mild steel corrosion in 1N hydrochloric acid with 4-amino-6-methyl-3-thi oxo-3,4-dihydro-1,2,4-triazin-5(2H)-one (AMTDT) and (4-amino-4H-1,2,4-triazole-3,5-diyl) dimethanol (ATD) was investigated by polarization (Tafel), electrochemical impedance (EIS), adsorption and computational calculations at 27 °C. The mixed type inhibitor property of these inhibitor molecules was investigated by potentiodynamic polarization studies. It was revealed that the effectiveness of inhibition is influenced by several factors such as the nature and state of the metal surface, the type of corrosive medium, the structure of the chemical compound used as inhibitor and molecular electronic parameters. Obvious correlations were found between corrosion inhibition efficiency and some quantum chemical parameters. Monte Carlo simulations were applied to search for the most stable configuration and adsorption energy for the interaction of inhibitors on Fe (1 1 1) interface. Calculated results indicated that the difference in inhibition efficiencies between the compounds can be clearly explained in terms of frontier molecular orbital theory.

1. Introduction

Generally, acid solutions are used for the removal of rust and scale in industrial processes. Inhibitors are used in these processes to control metal dissolution. Most of the well known inhibitors are organic compounds containing N, S, and or O atoms. Also, organic compounds containing functional electronegative groups and π electrons in triple or conjugated double bonds are used which enable them to adsorb to the metal surface and form protective complex layers. The study of corrosion processes and their inhibition by organic compounds is an active field of contemporary research [1–5]. Recently computational quantum chemical calculations and molecular simulation studies have also been used to explain the mechanism of corrosion inhibition [6–12]. The geometry of the inhibitor molecule in its ground state and the nature of their molecular orbitals (HOMO; Highest Occupied Molecular Orbital and LUMO; Lowest Unoccupied Molecular Orbital) are directly

* Corresponding author at: Department of Chemistry, University of Calicut, 673635 Kerala, India. Fax: +91 4812401472.
E-mail address: samthanicken@yahoo.com (S. John).
Peer review under responsibility of Egyptian Petroleum Research Institute.

http://dx.doi.org/10.1016/j.ejpe.2016.10.005

involved in the inhibitive properties of these molecules. The present investigation is an attempt to explore the corrosion inhibition action of 4-amino-6-methyl-3-thioxo-3, 4-dihydro-1,2,4-triazine-5(2H)-one (AMTDT) and (4-amino-4H-1,2,4-triazole-3,5-diyl) dimethanol (ATD) on mild steel in 1 M HCl by Tafel polarization and electrochemical impedance spectroscopy. The mechanism of inhibition was ascertained by scanning electron microscopy, adsorption studies and Monte Carlo simulation methods.

2. Experimental method

2.1. Inhibitor

About 170 ml of water was taken in a beaker and heated to boiling. Then, 23 g of thiocarbohydrazide and 14 g of pyruvic acid was added simultaneously. Light yellow crystals of 4-amino-6-methyl-3-thioxo-3,4-dihydro-1,2,4-triazine-5(2H)-one (AMTDT) formed were recrystallized from ethanol. The only method for the preparation of 1,2,4-triazole 4-amino-4H-1,2,4-triazole-3,5-dimethanol (ATD) is the condensation of glycolic acid with hydrazine hydrate. Hydrazine monohydrate (3.75 g, 0.75 mol) was added drop wise to 70% aqueous glycolic acid (54.3 g, 0.50 mol) at 0 °C. The resulting solution was heated at 120 °C for 6 h. Then, the reflux condenser was replaced with a downward condenser and the reaction mixture was heated at 160 °C for a further 18 h allowing excess hydrazine and water to distil off. After cooling, the resulting yellowish crystalline solid was recrystallized from water to give analytically pure ATD [9,10]. The geometries of the inhibitor molecules are shown in Fig. 1.

2.2. Medium

The medium for the study was prepared from reagent grade HCl (E. Merck) using double distilled water. All tests were performed in aerated medium at room temperature (300 K) and atmospheric pressure.

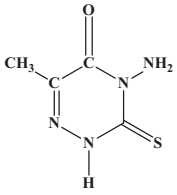

4-amino-6-methyl-3-thioxo-3,4-dihydro-1,2,4-triazin-5(2*H*)-one (AMTDT)

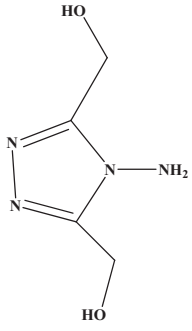

(4-amino-4*H*-1,2,4-triazole-3,5-diyl)dimethanol (ATD)

Figure 1 Structure of AMTDT and ATD.

2.3. Materials

The mild steel samples were of the following compositions (W%), C ≈ 0.2%; Mn ≈ 1%; P ≈ 0.03%; S ≈ 0.02%; Fe ≈ 98.75% as determined by Energy Dispersive Analysis of X-rays (EDAX) method (Fig. 2). For electrochemical studies mild steel specimens of 4.8 × 1.9 cm^2 coupons were used. But only 1 cm^2 area is exposed during each measurement. The samples were polished using different grades of emery papers (600–1200 grade) followed by washing with ethanol, acetone and finally with distilled water before each measurements as recommended by ASTM standard G-1-82.

2.4. Electrochemical measurements

Polarization and electrochemical impedance spectroscopy (EIS) measurements were carried out using Gill AC computer controlled electrochemical workstation (ACM, UK, model no: 1475). Electrochemical data were analyzed using Gill AC software. The excitation AC signal had amplitude 10 mV (RMS) in a frequency domain from 0.1 Hz to 10 kHz. The EIS were recorded after reaching a steady state open-circuit potential. The potentiodynamic polarization curves were obtained in the potential range from −250 mV to +250 mV with sweep rate of 1 mV/s. The scanning was carried out at a rate of 1 mV/s with respect to saturated calomel electrode (SCE). Prior to the potential sweep, the electrode was left under open circuit in the respective solution for approximately one hour until a steady free corrosion potential was recorded. Corrosion current density, I_{corr} which is equivalent to corrosion rate is given by the intersection of the Tafel line extrapolation. On the contrary, the current corresponding to the extrapolation at the corrosion potential of the first pseudo-linear part of the polarization curve coincides with I_{corr}, when the contribution of other currents in this region is negligible. Each experiment was repeated at least three times to check the reproducibility.

2.5. Computational studies

The use of quantum chemical calculations has become popular for screening new potential corrosion inhibitors [13]. The structural and electronic parameters of the compounds were calculated by molecular orbital theory in gaseous media. The

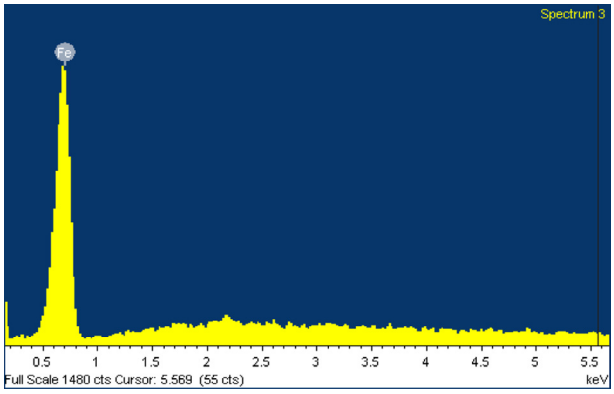

Figure 2 EDX spectrum of mild steel.

Please cite this article in press as: S. John et al., Corrosion inhibition properties of 1,2,4-Hetrocyclic Systems: Electrochemical, theoretical and Monte Carlo simulation studies, Egypt. J. Petrol. (2016), http://dx.doi.org/10.1016/j.ejpe.2016.10.005

GAUSSIAN-03 W program, SCRF methods (self-consistent reaction field) were used for the calculations. All the geometries of the inhibitor were optimized using B3LYP/6-311G* basis set. The most popular parameters which play a prominent role are involved in the hard–soft acid–base (HSAB) theory of chemical reactivity. These involve the Eigen values of the HOMO and LUMO, the HOMO–LUMO gap (ΔE), chemical hardness/softness, electronegativity and the number of electrons transferred from the inhibitor molecule to the metal surface. Molecular dipole moments and Fukui functions are also frequently used in corrosion inhibition studies.

The local reactivity of the inhibitor molecule was analyzed through an evaluation of the Fukui indices. Fukui indices are a measure of the chemical reactivity, as well as an indicative of the reactive regions and the nucleophilic and electrophilic behaviors of the molecule. The regions of a molecule where the Fukui function is large are chemically softer than the regions where the Fukui function is small, and by invoking the HSAB principle in a local sense, one may establish the behavior of different sites with respect to hard or soft reagents. The Fukui function $f(\vec{r})$ is defined as the derivative of the electronic density $\rho(\underset{r}{\rightarrow})$ with respect to the number of electrons N at a constant external potential $\sigma(\underset{r}{\rightarrow})$

$$f(\vec{r}) = \left(\frac{\partial \rho(\underset{r}{\rightarrow})}{\partial N}\right)_{\sigma(\underset{r}{\rightarrow})} \tag{1}$$

If the effects of relaxation associated with the addition or removal of electronic charges are not considered, then

$$\rho^{+}(\vec{r}) \approx \rho_{\mathrm{LUMO}}(\vec{r}) \tag{2}$$

$$\rho^{-}(\vec{r}) \approx \rho_{\mathrm{HOMO}}(\vec{r}) \tag{3}$$

where $\rho_{\mathrm{LUMO}}(\vec{r})$ is the density of the lowest unoccupied molecular orbital and $\rho_{\mathrm{HOMO}}(\vec{r})$ is density of the highest occupied molecular orbital [14–17]. The condensed Fukui functions are found by taking the finite difference approximations from Mulliken population analysis of atoms in the inhibitor, depending on the direction of the electron transfer.

$$f_k^{+} = \mathrm{q_k(N+1)} - \mathrm{q_k(N)} \tag{4}$$

$$f_k^{-} = \mathrm{q_k(N)} - \mathrm{q_k(N-1)} \tag{5}$$

where q_k is the gross charge of atom k in the molecule i.e. the electron density at a point 'r' in space around the molecule. The N corresponds to the number of electrons in the neutral molecule, $N + 1$ corresponds to an anion, with an electron added to the LUMO of the neutral molecule and $N - 1$ represents the cation with an electron removed from the HOMO of the neutral molecule. All calculations are done at the ground-state geometry. These functions can be condensed to the nuclei using an atomic charge partitioning scheme, such as Mulliken population analysis in Eqs. (2)–(5). An easy graphical display technique was also used based on the Fukui functions. Instead of calculating the molecular orbitals for the neutral, cation, and anion, one can just add or subtract electrons from the molecular orbitals of the neutral molecule. Though this procedure is not as good as the first method, it does give a quick graphical display of the susceptibility of different kinds of attack.

2.6. Molecular simulation study

Molecular simulation studies were performed using Materials studio 4. 3 software from Accelrys Inc. [14]. It has been used to build the inhibitor molecules on mild steel surface. The key approximation is that the potential energy surface, on which the atomic nuclei move, is represented by a classical forcefield. COMPASS (Condensed-phase Optimized Molecular Potentials for Atomistic Simulation Studies) [15] is the first ab initio forcefield that enables accurate and simultaneous prediction of chemical properties (structural, conformational, vibrational, etc.) and condensed-phase properties (equation of state, cohesive energies, etc.) for a broad range of chemical systems. It is also the first high quality forcefield to consolidate parameters of organic and inorganic materials.

The first step in this computational study is the preparation of a model of molecules which adsorb on the surface with optimized geometry (i.e. energy minimized). Among the different steps involved in the modeling approach, is the construction of the iron surface from its pure crystal, the addition of the inhibitor near to the surface, followed by the geometry optimization calculation. Once the model has been optimized with suitable forcefield (COMPASS), we will be able to simulate a substrate loaded with an adsorbate.

The objective of this computational study is to find the nearer inhibitor molecule to Fe (1 1 1) surface. The MD simulation of the interaction between compound and iron surface was carried out in a simulation box with periodic boundary conditions to model a representative part of the interface devoid of any arbitrary boundary effects. The iron plane was first built and relaxed by minimizing its energy using molecular mechanics, after minimizing the mild steel surface and ligand molecule, the corrosion system will be built by layer builder to place the inhibitor molecules on iron surface, and the behaviors of the these molecules on the iron surface were simulated using the COMPASS (condensed phase optimized molecular potentials for atomistic simulation studies) force field. Adsorption Locator module in Materials Studio 4.3 has been used to model the adsorption of the inhibitor molecules on to mild steel surface and thus provides access to the energetic of the adsorption and its effects on the inhibition efficiencies of inhibitor molecule [18].

2.7. Scanning electron microscopy (SEM)

The surface morphology of the sample under study in the absence and presence of inhibitors was carried out using a scanning electron microscope model SU6600 (Serial No: HI-2102-0003) with an accelerating voltage of 20.0 kV. Samples were attached on the top of an aluminum stopper by means of carbon conductive adhesive tape. All micrographs of the specimen were taken at the magnification of 500×.

3. Results and discussion

3.1. Potentiodynamic polarization studies

Polarization measurements have been carried out to pool information concerning the kinetics of anodic and cathodic reaction. Potentiodynamic polarization curves for mild steel in 1N HCl solution in the absence and presence of various

concentrations of the inhibitor molecule are shown in Fig. 3. The values of electrochemical kinetic parameters like corrosion current density (I_{corr}) and Tafel slopes (β_a and β_c), determined from these graphs by extrapolation method, are listed in Table 1. The corrosion inhibition efficiency (IE) was calculated using the relation

$$\%IE = \frac{\mathbf{I_{corr^*}} - \mathbf{I_{corr}}}{\mathbf{I_{corr^*}}} \times 100 \quad (6)$$

where I_{Corr^*} and $\mathbf{I_{corr}}$ are uninhibited and inhibited corrosion current density respectively determined by extrapolation of Tafel lines in the corrosion potential. In acidic solutions, the anodic reaction of corrosion is the passage of metal ions from the metal surface into the solution, and the cathodic reaction is the discharge of hydrogen ions to produce hydrogen gas or to reduce oxygen. The inhibitor may affect either the anodic or the cathodic reaction, or both. Inspection of Fig. 3, shows that the addition of inhibitor has an inhibitive effect on both anodic and cathodic parts of the polarization curves and shifts both the anodic and cathodic curves to lower current densities. This may be ascribed to adsorption of the inhibitor over the metal surface. Therefore, inhibitor AMTDT and ATD can be considered as a mixed type inhibitor.

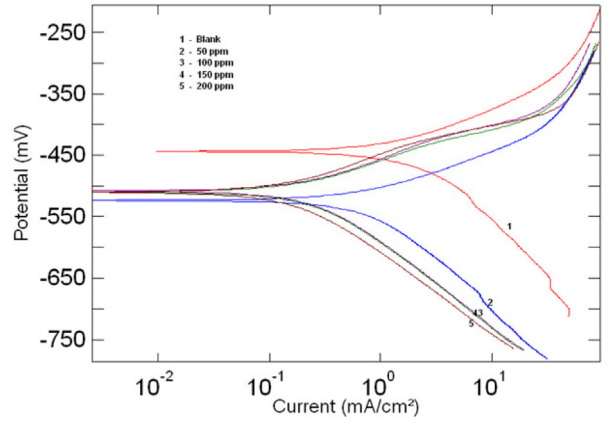

(a)

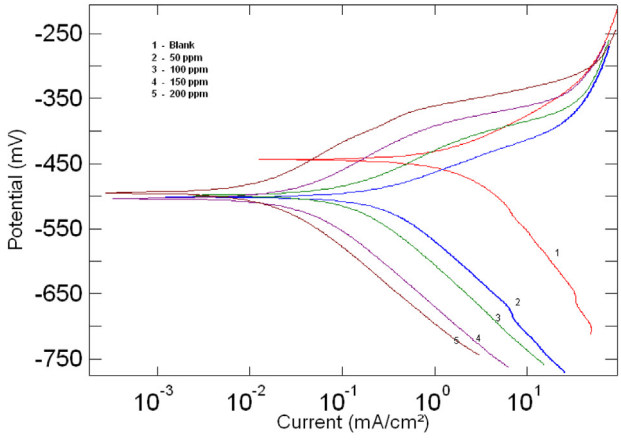

(b)

Figure 3 Anodic and cathodic Tafel lines for mild steel in uninhibited 0.1 N HCl and with different concentrations of inhibitor: (a) AMTDT and (b) ATD.

The cathodic branch of polarization curve gives rise to parallel lines with the increasing inhibitor concentration while cathodic corrosion current density decreased considerably. This reveals that the addition of AMTDT and ATD does not change the cathodic hydrogen evolution mechanism and the decrease of H^+ ions on the metal surface take place mainly through a charge transfer mechanism. The suppression of the cathodic process can be attributed to the adsorption of inhibitor molecules on cathodic sites. Thus, addition of this inhibitor reduces the iron dissolution as well as delaying the hydrogen evolution reactions. In the anodic branch of polarization curve the inhibitor molecule first adsorb on the iron surface and blocking the available reaction sites [19]. The surface coverage increases with inhibitor concentration. The formation of surface inhibitor film on iron surface reduces the active surface area available for the attack of the corrosive media and delays hydrogen evolution and metal dissolution and provides considerable protection to mild steel against corrosion [17]. The corrosion parameters derived from these curves are listed in Table 1. It is clearly seen that the corrosion current density (I_{corr}) and corrosion rate (CR) value decrease considerably with increasing concentration of the inhibitor due to the formation of a barrier film on the steel surface, while inhibition efficiency increases with inhibitor concentration, and maximum IE% is up to 94.28 of AMTDT and 94.44 of ATD at 200 ppm .

3.2. Electrochemical impedance spectroscopy

Impedance measurements were made under potentiostatic conditions after 1hour of immersion. Nyquist plots of uninhibited and inhibited solution containing different concentrations of inhibitor molecule are performed over a frequency range from 0.1 Hz to 10,000 Hz and are shown in Fig. 4a. The similarity in the shapes of these graphs throughout the experiment, indicates that the addition of inhibitor molecule does not make any change in the corrosion mechanism. The corresponding Bode plots are shown in Fig. 4b. The capacitive loop at high frequencies represents the phenomenon associated with electrical double layer. The above impedance diagrams (Nyquist) contain depressed semicircles with the center under real axis. Such behaviors are characteristic of solid electrode and often referred to frequency dispersion attributed to different physical phenomenon such as roughness, inhomogeneities of the solid surfaces, impurities, grain boundaries, and distribution of surface active sites. The ideal capacitive behavior is not seen in this case and hence a constant phase element CPE is introduced in the circuit to give a more accurate fit [20–22]. The simplest fitting is represented by Randles equivalent circuit (Fig. 5), which is a parallel combination of the charge-transfer resistance (R_{ct}) and the constant phase element (CPE), both in series with the solution resistance (R_s). The impedance function of a CPE can be represented as

$$Z_{CPE} = A^{-1}(j\omega)^{-n} \quad (7)$$

where A is the CPE constant (in $\Omega^{-1}\,S^n\,cm^{-2}$), $i^2 = -1$, ω is the angular frequency ($\omega = 2\pi f$ where f is the angular frequency) and n is the CPE component which give details about the degree of surface inhomogeneity [23,24]. Evaluation of

Table 1 Polarization parameter and corresponding inhibition efficiency for the corrosion of mild steel in 0.1 N HCl at various concentrations of AMTDT and ATD.

Inhibitor	Conc (ppm)	E_{corr} (mV)	LPR (Ω cm^2)	β_a (mV dec^{-1})	$-\beta_c$ (mV dec^{-1})	I_{corr} (mA cm^{-2})	C.R (mm/yr)	η (%)
Blank	–	−445	4.3107	111	197	3.001	34.781	–
AMTDT	50	−523	5.1665	89	195	1.3635	15.803	54.56
	100	−509	5.1244	69	157	0.4174	4.8382	86.09
	150	−507	5.5578	66	150	0.3176	3.6811	89.41
	200	−509	6.6214	56	129	0.1716	1.9891	94.28
ATD	50	−461	7.65	120	169	2.1290	24.68	29.05
	100	−460	7.90	100	145	1.5967	18.51	46.79
	150	−475	18.04	80	113	0.4020	4.65	86.60
	200	−478	23.41	79	94	0.1666	1.93	94.44

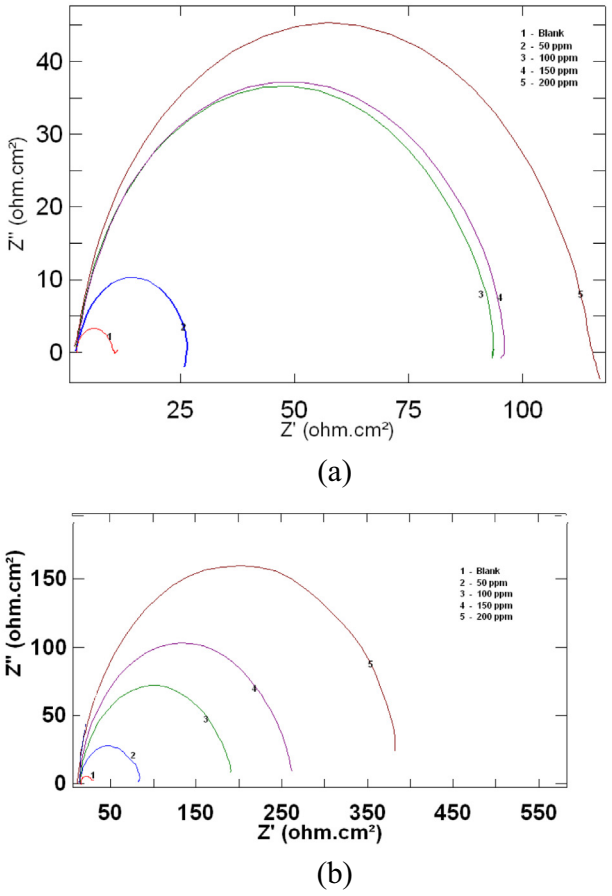

Figure 4a Nyquist plots for mild steel in uninhibited 0.1 N HCl and with different concentrations of inhibitor: (a) AMTDT and (b) ATD.

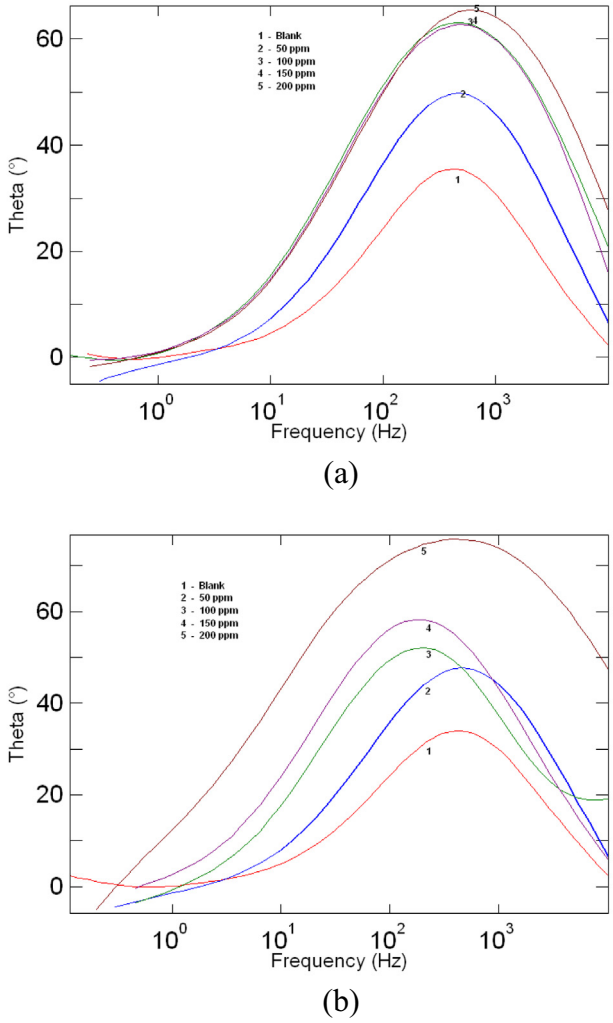

Figure 4b Bode plots for mild steel in uninhibited 0.1 N HCl and with different concentrations of inhibitor: (a) AMTDT and (b) ATD.

Table 2 shows that the values of R_{ct} and C_{dl} have opposite trend at the whole concentration range and it may be due to the formation of a protective layer on the surface of the electrode. The double layer between the charged metal surface and the solution is considered as an electrical double capacitor. The adsorption of inhibitor molecule on mild steel surface decreases its electrical capacity through the displacement of water molecule and other ions originally adsorbed on the metal surface [24]. The increase in the thickness of the protective layer and decrease in the value of C_{dl} with increase in inhibitor

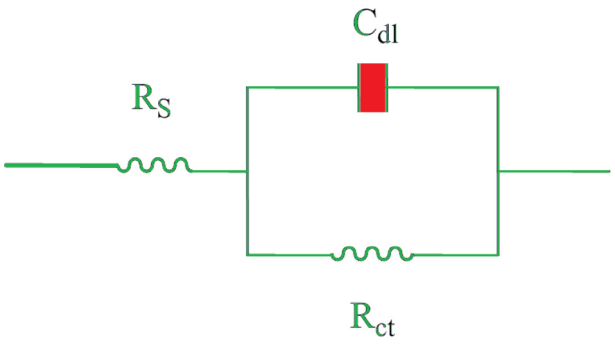

Figure 5 Equivalent circuits used to fit for the EIS data mild steel in 0.1 N HCl and with different concentrations of inhibitor.

concentration shows the inhibitor molecule electrostatically adsorbs on the electrode surface. This trend is in accordance with the Helmholtz model given by the equation

$$C_{dl} = \frac{\Sigma\Sigma_0 A}{d} \quad (8)$$

where d is the thickness of the protective layer, $\sum$ is the dielectric constant of the medium, Σ_0 is the vacuum permittivity and A is the surface area of the electrode.

The equation used for calculating the percentage corrosion inhibition efficiency (IE) is

$$\%IE = \frac{\mathbf{R_{ct^*}} - \mathbf{R_{ct}}}{\mathbf{R^*_{ct}}} \times 100 \quad (9)$$

where $\mathbf{R_{ct}}^*$ and $\mathbf{R_{ct}}$ are values of the polarization resistance observed in the presence and absence of inhibitor molecule. Impedance parameters are summarized in Table 2.

3.3. Adsorption studies

The selection of these inhibitor molecules are based on their mechanism of action, for example their ability to donate electrons. The adsorption of inhibitor at an electrode/electrolyte interface may take place through displacement of adsorbed water molecules at the inner Helmholtz plane of the electrode, likely in agreement with the following equation:

$$Org_{aq} + X \cdot H_2O_{ads} \leftrightarrow Org_{ads} + X \cdot H_2O_{aq}$$

where X, the size ratio, is the number of water molecules displaced by one organic inhibitor molecule. Adsorption plays a significant role in the inhibition of metallic corrosion by organic molecules. Attempts were made to fit the θ values to various isotherms, including Langmuir, Temkin, Frumkin and Flory-Huggins. By far, the best fit is obtained with Langmuir isotherm [23,24]. The Langmuir isotherm gives a straight-line graph for the plot of C/θ vs C. The straight line obtained for the inhibitor molecule is given in Fig. 6. The strong correlations (R^2 = 0.9427 and 0.9894) confirm the validity of this approach [25].

3.4. Quantum chemical calculations

The molecular sketches of the inhibitor were drawn using Gauss View 5.0. All the quantum chemical calculations were performed with complete geometry optimization using standard Gaussian 03 software package. Geometry optimization and quantum chemical calculations performed using Density Functional Theory (DFT). The Becks three parameter hybrid functional was combined with the Lee, Yang and Parr (LYP) correlation functional and denoted as B3LYP and was employed in the DFT calculations using 6-311G* basis set.

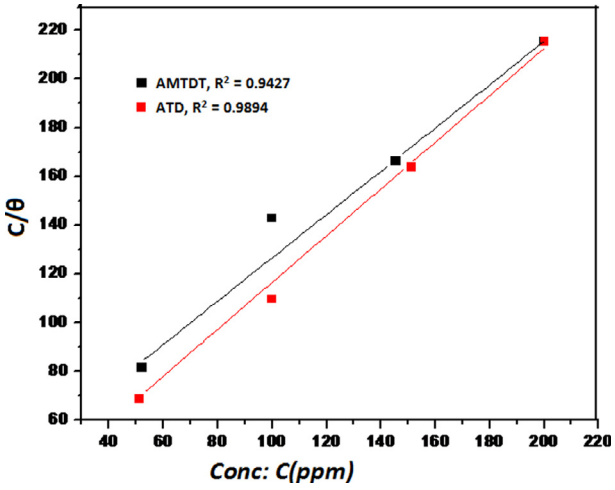

Figure 6 Langmuir adsorption isotherms for the inhibitor.

Table 2 Impedance parameter for the corrosion of mild steel in 0.1 N HCl at various concentrations of AMTDT and ATD.

Inhibitor	Conc. (ppm)	R_{ct} (μF cm^{-2})	C_{dl} (μA cm^2)	R_{soln} (Ω cm^2)	n	η (%)
Blank	–	8.05	562.60	6.547	0.80	–
AMTDT	50	25.20	152.10	11.321	0.88	68.05
	100	93.07	96.49	18.674	0.85	91.34
	150	95.71	95.05	33.938	0.84	91.58
	200	113.43	66.08	48.452	0.86	92.90
ATD	50	24.77	208.50	10.563	0.87	67.50
	100	26.92	203.30	17.045	0.87	70.01
	150	100.00	88.60	31.970	0.90	91.95
	200	113.31	84.50	46.827	0.90	92.89

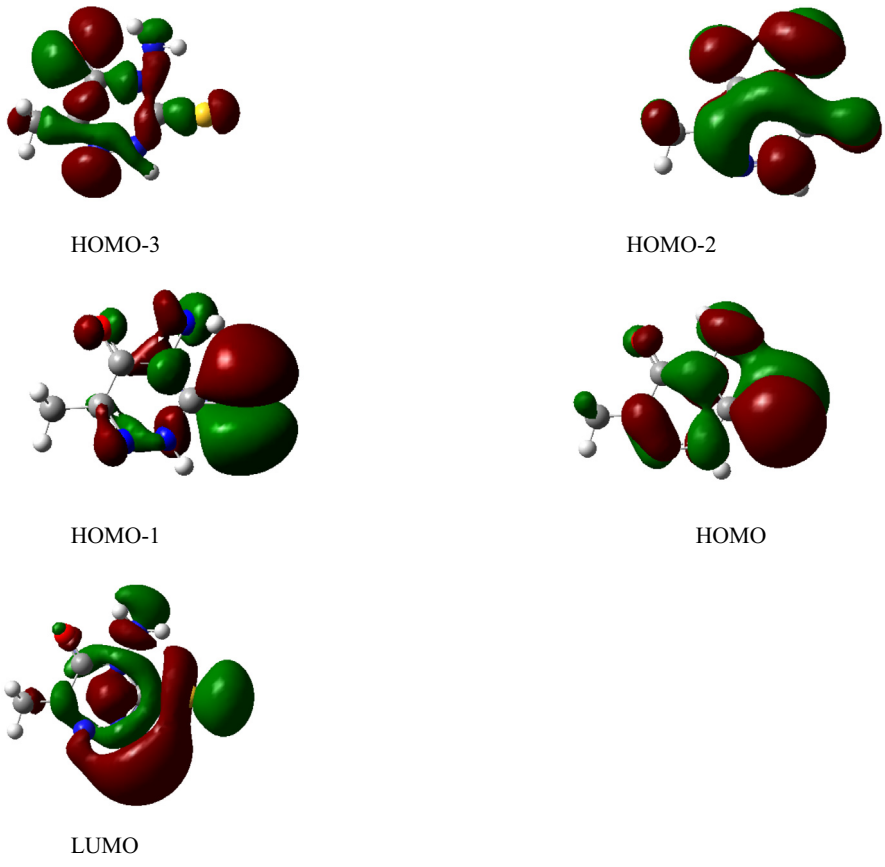

(a)

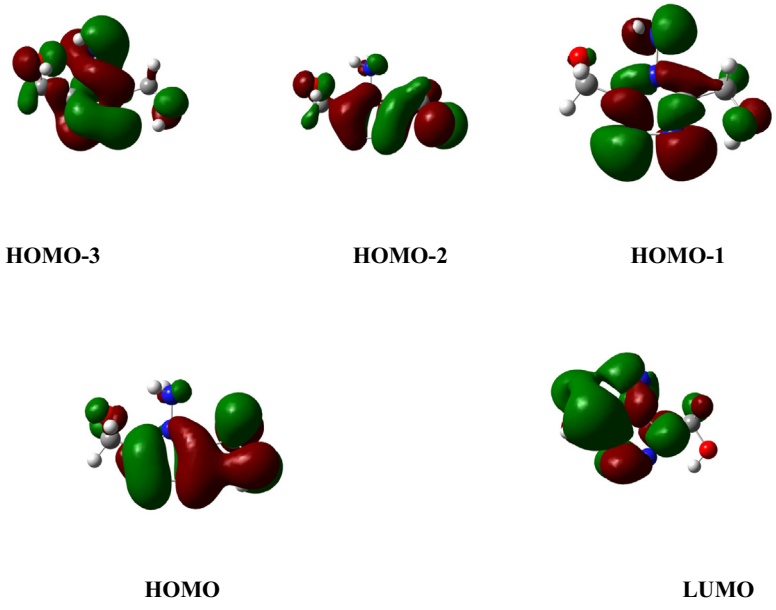

(b)

Figure 7 Frontier molecular orbitals of (a) AMTDT and (b) ATD in particular HOMO-3, HOMO-2, HOMO-1, HOMO and LUMO are plotted; Label HOMO-n stands for *n*th MO below the HOMO. The isosurface of $\pm 0.04(e/bohr^3)^{1/2}$.

Table 3 The calculated quantum chemical properties of AMTDT and ATD.

Inhibitor	HOMO (eV)	LUMO (eV)	ΔE (eV)	μ	I	A	χ	η	ΔN
AMTDT	−2.3578	−6.4997	4.1419	1.9863	2.3578	6.4997	4.4287	2.0709	0.6207
ATD	−0.1382	−6.9805	6.8423	4.9367	0.1382	6.9805	3.5504	3.4212	0.5028

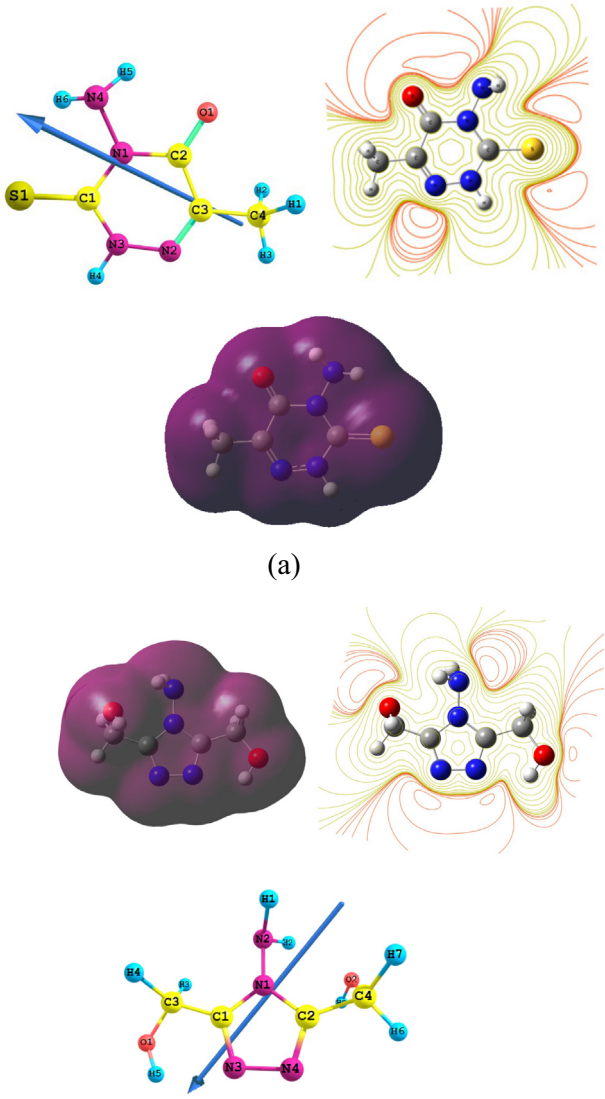

Figure 8 Electrostatic properties of (a) AMTDT and (b) ATD: side views of the dipole are displayed on the left while the middle and right panels show the contour and isosurface representation of electrostatic potential respectively.

Molecular orbitals are designated with respect either to HOMO or LUMO orbital [26–29]. The label HOMO-n stands for *n*th orbital below the HOMO and LUMO orbitals shown in Fig. 7. There are two different definitions used for the chemical hardness, ŋ, that differ by a factor of two [30]. This affects all other electronic parameters that depend on ŋ. We use the definition based on the following two equations;

$$\mu = \frac{\partial E}{\partial N} \quad \text{and} \quad \eta = \frac{1}{2}\frac{\partial^2 E}{\partial N^2} \tag{10}$$

where E is the total energy of the system, N is the number of electrons, and μ is the electronic chemical potential. The other definition drops the factor 1/2 from the definition of ŋ. The HSAB parameters can be derived by Eq. (5) using finite difference approximation for the first and second Eigen values of HOMO and LUMO, $-E_{HOMO}$ and $-E_{LUMO}$, for the ionization potential and electron affinity [31,32]. The electronegativity, χ, is the negative of chemical potential and hence given by

$$\chi = -\mu \approx -1/2(E_{HOMO} + E_{LUMO})$$

while chemical hardness, ŋ is approximated by

$$\eta \approx 1/2(E_{HOMO} - E_{LUMO})$$

The work function Φ of the metal surface is taken as electronegativity; whereas chemical hardness is neglected, because ŋ of bulk metal is inverse of their density state at the Fermi level which is an exceedingly small number. The number of electrons transferred from the molecule to metal ΔN, will be given by

$$\Delta N = \frac{(\chi_{Fe} - \chi_{inhi})}{2(\eta_{Fe} - \eta_{inhi})} \tag{11}$$

where Fe is considered as Lewis acid according to HSAB concept [33]. The difference in electronegativity drives the electron transfer, and the sum of the hardness parameters act as a resistance. In order to calculate the fraction of electrons transferred, a theoretical value for the electronegativity of bulk metal was used $\chi_{Fe} \approx 7$ eV, and a global hardness of $\eta_{Fe} \approx 0$, by assuming that for a metallic bulk I = A [34,35] because they are softer than the neutral metallic atoms. Some of the calculated electronic parameters like the highest occupied (E_{HOMO}) and lowest unoccupied (E_{LUMO}) molecular orbital energies, the energy gap ($\Delta E = E_{LUMO} - E_{HOMO}$), and the dipole moment are presented in Table 3. E_{HOMO} is often associated with the electron donating ability of inhibitor molecule to the unoccupied d orbital of metal. Thus, the less negative values of E_{HOMO} and, similarly, the lower value of the gap energy should both increase the effectiveness of inhibition. The low value of dipole moment has often been associated with good inhibition properties [36–39]. The direction of the dipole can be understood by considering the electrostatic potential (middle and right panels of Fig. 8). Dipole moments are substantially enhanced for both inhibitors on going from the gaseous to the aqueous phase, indicating an increase in the stability of the inhibitors due to the interaction with water. The local reactivity was analyzed by means of the condensed Fukui function. The condensed Fukui functions allow us to

Table 4 Fukui functions and local softness values for a nucleophilic and electrophilic for AMTDT & ATD.

AMTDT					ATD				
Atom	f^-	f^+	Sk^-	Sk^+	Atom	f^-	f^+	Sk^-	Sk^+
1C	0.0407	0.0412	0.0842	0.0853	1C	0.0268	0.2664	0.0212	0.2108
2N	0.0181	0.0940	0.0374	0.1946	2C	0.0265	0.2675	0.0209	0.2116
3C	0.0018	0.1352	0.0372	0.2798	3N	0.2039	0.2025	0.1613	0.1602
4C	0.0032	0.2366	0.0066	0.4898	4H	0.4807	0.0425	0.3803	0.0336
5N	0.0126	0.2880	0.026	0.5962	5H	0	0	0	0
6O	0.0098	0.1051	0.0203	0.2175	6H	0	0	0	0
7C	0.0012	0.0025	0.0024	0.0052	7N	0.1181	0.0524	0.0934	0.0414
8H	0	0.0077	0	0.0159	8N	0.1186	0.0531	0.0938	0.0420
9H	0.0006	0.0078	0.0012	0.0161	9C	0.0009	0.0122	0.0007	0.0096
10H	0.0002	0	0.0004	0	10H	0.0032	0.0225	0.0025	0.0178
11N	0.0115	0.0347	0.0238	0.0718	11H	0.0032	0.0225	0.0025	0.0178
12H	0.0034	0	0.0071	0	12O	0.0053	0.0006	0.0042	0.0004
13N	0.0960	0.0120	0.1987	0.0248	13H	0	0	0	0
14S	0.7916	0.0292	1.6387	0.0604	14H	0.0009	0.0123	0.0007	0.0097
15H	0.0009	0.0040	0.0018	0.0082	15H	0.0032	0.0225	0.0025	0.0178
					16H	0.0032	0.0226	0.0025	0.0021
					17O	0.0053	0.0006	0.0042	0.0004
					18H	0	0	0	0

Table 5 The outputs and descriptors calculated by Monte Carlo simulation for adsorption of inhibitor on Fe (1 1 1) plane.

Inhibitor	Total energy (kJ mol^{-1})	Adsorption energy (kJ mol^{-1})	Rigid ad energy (kJ mol^{-1})	Deformation energy (kJ mol^{-1})	Atomistic: dEad/dNi
ATD	44.4	−14472.4	5.04	−14472.4	−14472.4
AMTDT	66.4781	−90809.3	2.08	−90809.3	−90809.3

distinguish each part of the molecule on the basis of its distinct chemical behavior due to different functional groups or substituents. Thus, the site for nucleophilic attack will be the place where the value of f_k^+ is a maximum and the site for electrophilic attack will be the place where the value of f_k^- is maximum. The values of the Fukui functions for a nucleophilic and electrophilic attack are given in Table 4 (only for the nitrogen, oxygen, sulfur and carbon atoms). Inspection of the values of Fukui functions presented in Table 4 shows that the inhibitor AMTDT and ATD has propitious zones for nucleophilic attack located on AMTDT (3C, 4C, and 5N), and ATD (1C and 2C) while electrophilic attack has on AMTDT (13N and 14S) and on ATD (3N and 4H). Data in Table 4 also show that AMTDT has more susceptible sites for adsorption on the metal surface, which reflects its highest inhibition performance. The HOMO location on each system agrees with the atoms that exhibit greatest values of indices of Fukui, both indicate the zones by which the molecule would be adsorbed on the mild steel surface.

3.5. Monte Carlo simulation study

Molecular modeling studies give more insight into the nature of attraction between iron and inhibitor AMTDT and ATD. The modeling studies were designed to examine this theory by predicting the inhibitor–surface interactions that lead to optimal molecular binding at the mild steel surface. Monte Carlo, molecular dynamics simulation was performed on a system comprising AMTDT and ATD and iron surface. Inhibitor is firstly placed on the iron surface, optimize and then run molecular dynamics. The Monte Carlo simulation process tries to find the lowest energy for the whole system. The structures of the adsorbate components are minimized until they satisfy certain specified criteria. The outputs and descriptors calculated by the Monte Carlo simulation are presented in Table 5. The parameters presented in Table 5 include total energy of the substrate–adsorbate configuration. The total energy is defined as the sum of the energies of the adsorbate components, the rigid adsorption energy, and the deformation energy. In this study, the substrate energy (steel surface) is taken as zero. Also, adsorption energy reports energy released (or required) when the relaxed adsorbate components are adsorbed on the substrate. The adsorption energy is defined as the sum of the rigid adsorption energy and the deformation energy for the adsorbate components. The rigid adsorption energy, reports the energy, in kcal mol^{-1}, released (or required) when the unrelaxed adsorbate components (i.e., before the geometry optimization step) are adsorbed on the substrate. The deformation energy, reports the energy released when the adsorbed adsorbate components are relaxed on the substrate surface. Table 5 shows also, (dE_{ads}/dNi) which defines the energy of substrate–adsorbate configurations where one of the adsorbate components has been removed. High values of adsorption energy confirm experimental results and explain why the amino derivative gives the highest inhibition effi-

ciency. The "total energy" of a molecule presented in Table 5 refers to the energy of a specific arrangement of atoms. The zero energy reference is taken to be the infinite separation of all electrons and nuclei, so the total energy is generally negative, corresponding to a bound state. Fig. 9 shows the predicted adsorption density of AMTDT and ATD on the mild steel surface. As can be seen from Table 5 the adsorption of inhibitor shows the highest ability to adsorb on Fe (1 1 1) surface with highest adsorption energy. Also, it has the highest binding energy to iron surface as seen in Table 5. Adsorption density calculation presented in Fig. 9 is identified by carrying out a Monte Carlo search of the configurational space of the substrate–adsorbate system. This process is repeated to identify further local energy minima. During the course of the simulation, adsorbate molecules are randomly rotated and translated around the substrate. The configuration that results from one of these steps is accepted or rejected according to the selection rules of the Metropolis Monte Carlo method.

3.6. Scanning electron microscopy (SEM)

Surface examination using SEM was carried out to understand the effect of inhibitor molecule on the surface morphology of mild steel. Fig. 10a shows the SEM image of a polished mild steel surface. Fig. 10b shows SEM image of the surface of mild steel after immersion in acid without inhibitor molecule for 48 h. This micrograph shows the effect of acid on surface damage. Fig. 10c shows SEM image of the surface of mild steel immersed in acid solution containing 200 ppm of AMTDT and ATD. So it can be concluded that corrosion is much less in the presence of inhibitors and the appearance of more polished surface obtained which proves its higher inhibition efficiency.

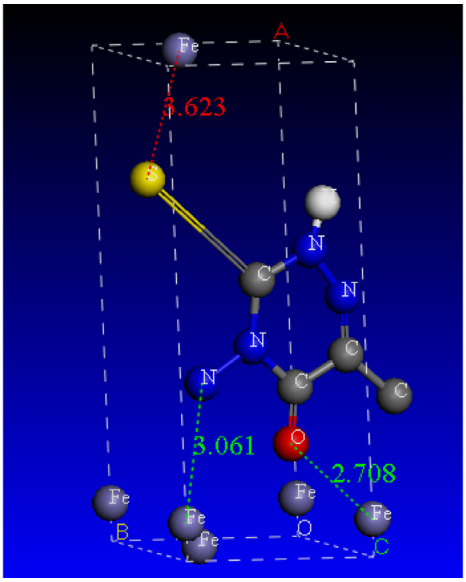

(a)

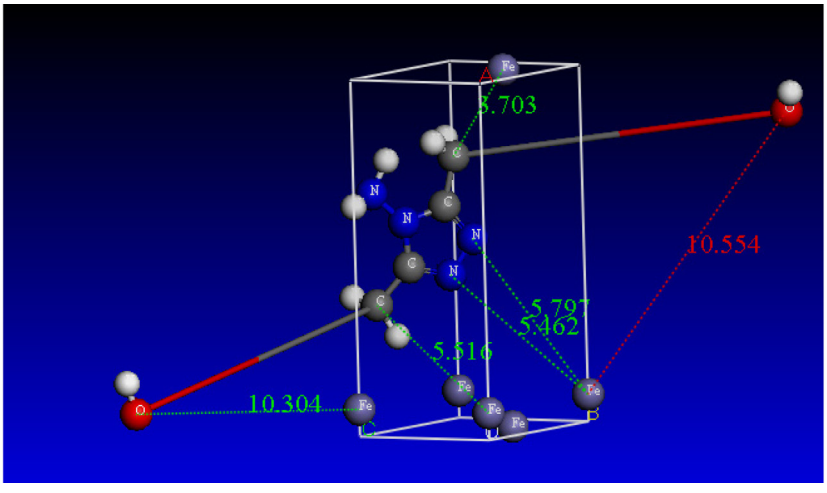

(b)

Figure 9 Modes of adsorption of (a) AMTDT and (b) ATD on Fe (1 1 1) plane.

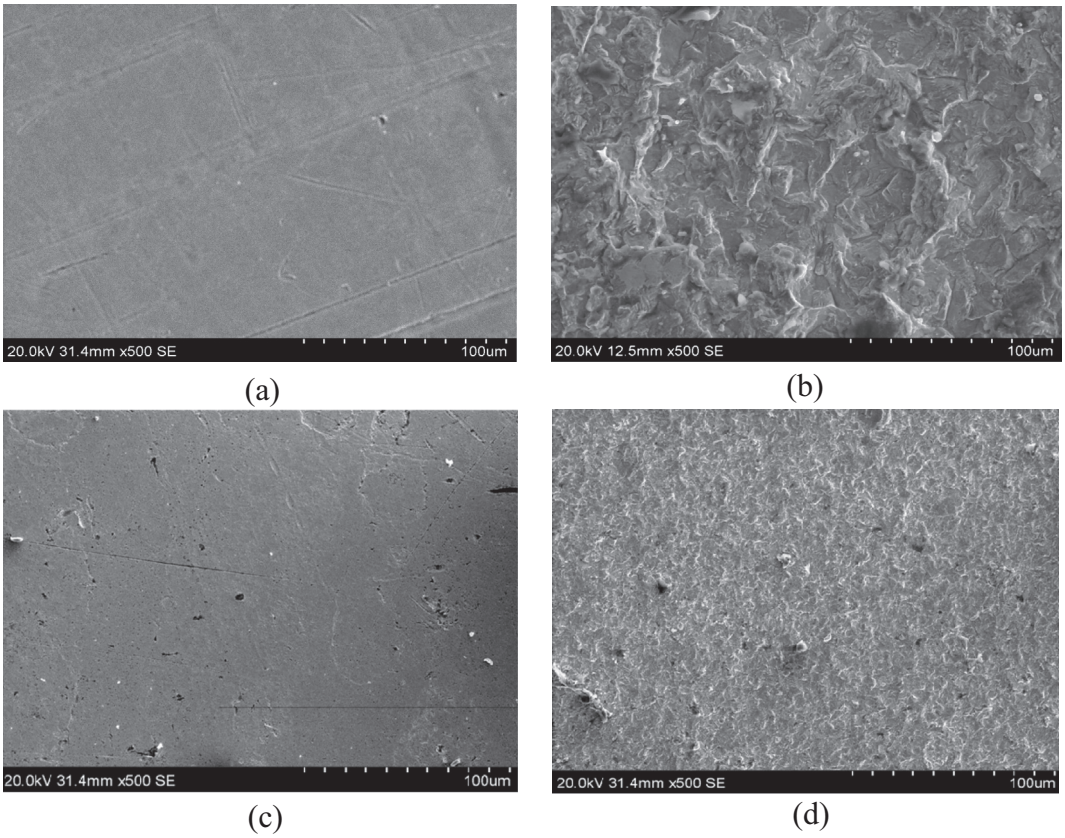

Figure 10 SEM images of (a) blank mild steel, (b) in 0.1 N HCl without inhibitor, (c) in the presence of 200 ppm of AMTDT after 48 h, and (d) in the presence of 200 ppm of ATD after 48 h.

4. Conclusions

(a) The inhibitor molecules show very good inhibitive efficiency for mild steel in 1 M HCl.
(b) The polarization plots indicated that the compounds act as mixed type inhibitors which inhibit both anodic metal dissolution and cathodic hydrogen evolution reaction.
(c) EIS plots indicated that the inhibitor increases the charge transfer resistance, and the inhibitive performance depends on the adsorption of the triazine derivatives on the metal surface.
(d) The inhibitive action of AMTDT and ATD follows Langmuir adsorption isotherm.
(e) The fraction of electrons transferred, ΔN, cannot be taken as a direct theoretical measurement of the inhibition efficiency. Hence change in the geometry of the molecule during adsorption is also considered theoretically and these values agree reasonably well with experimental results.
(f) The inhibitor molecules adsorb on the metal surface and block the reaction sites. Higher surface coverage on the metal surface was obtained with higher inhibitor concentrations. Scanning Electron Microscopy results also confirm the adsorption of inhibitor molecules on the metal surface.
(g) From Monte Carlo simulation studies it is clear that the inhibitor AMTDT is nearer to the surface of Fe (1 1 1) plane.
(h) At higher concentration of the inhibitor, both the inhibitor AMTDT and ATD have almost same inhibition efficiency, but at lower concentration the inhibitor AMTDT had greater efficiency than ATD.

References

[1] S. John, B. Joseph, K.K. Aravindakshan, A. Joseph, Mater. Chem. Phys. 122 (2010) 374–379.
[2] S. John, B. Joseph, K.V. Balakrishnan, K.K. Aravindakshan, A. Joseph, Mater. Chem. Phys. 123 (2010) 218–224.
[3] A. Fiala, A. Chibani, A. Drchen, A. Boulkam, K. Djebbar, Appl. Surf. Sci. 253 (2007) 9347–9356.
[4] F. Zucchi, G. Trabanelli, C. Monticelli, Corros. Sci. 38 (1996) 147–154.
[5] J.P. Chopart, J. Douglade, P. Fricoteaux, A. Olivier, Electrochim. Acta 36 (1991) 459–463.
[6] M.D. Pritzker, T.Z. Fahidy, Electrochim. Acta 37 (1992) 103–112.
[7] S. Magiano, Electrochim. Acta 42 (1997) 377–382.
[8] S. Krzewska, Electrochim. Acta 42 (1997) 3531–3540.
[9] H. CPyun, S.M. Park. J. Electrochem. Soc. 133 (1986) 2024–2030.
[10] E.E. Oguize, Y. Li, S.G. Wang, F. Wang, RSC. Adv. 1 (2011) 866–873.
[11] J.M. Bastidas, J.D. Damborenea, A.J. Vazquez, J. Appl. Electrochem. 27 (1997) 345–349.
[12] A.M. Fekry, M.A. Ameer, Int. J. Hydro. Energy 36 (2011) 11207–11215.

[13] M.H. Klingele, B. Moubaraki, K.S. Murray, S. Brooker, Chem. Eur. J. 11 (2005) 6962–6973.
[14] M. Cossi, M. Barone, R. Cammi, J. Tomassi. Chem. Phys. Lett. 255 (1996) 327–335.
[15] T. Arslan, F. Kandemirli, E.E. Ebenso, I. Love, H. Alemu, Corros. Sci. 51 (2009) 35–47.
[16] G. Gece, Corros. Sci. 50 (2008) 2981–2992.
[17] R. Solmaz, G. Kardas, M. Culha, B. Yazici, M. Erbil, Electrochim. Acta 53 (20) (2008) 5941–5952.
[18] M. Labjar, N. Lebrini, F. Bentiss, N.E. Chihib, S.E. Hajjaji, C. Jama, Mater. Chem. Phys. 119 (2010) 330–336.
[19] E.E. Ebenso, T. Arslan, F. Kandemirli, N. Caner, I. Love, Int. J. Quantum Chem. 110 (2009) 1003–1018.
[20] M.A. Amin, S.S. AbedEl-Rehim, E.E.F. El-Sherbini, R.S. Bayyomi, Electrochim. Acta 52 (11) (2007) 3588–3600.
[21] M.A. Veloz, I. Gonzalez, Electrochim. Acta 48 (2002) 135–144.
[22] E.M. Sherif, S.M. Park, Electrochim. Acta 51 (2006) 1313–1321.
[23] R. Macdonald, D.R. Franceshetti, Impedance Spectroscopy, Wiley, New York, 1987.
[24] M. Outirite, M. Lagrenee, M. Lebrini, M. Traisnel, C. Jama, H. Vezin, F. Bentiss, Electrochim. Acta 55 (2010) 1670–1681.
[25] A.A. El-Awady, B.A. Abd-El-Nabey, S.G. Aziz, J. Electrochem. Soc. 139 (1992) 2149–2154.
[26] M.A. Ameer, A.M. Fekry, Int. J. Hydro. Energy 35 (2010) 11387–11396.
[27] E.E. Ebenso, I.B. Obot, L.C. Murulana, Int. J. Electrochem. Sci. 5 (2010) 1574–1586.
[28] M.K. Awad, R.M. Issa, F.M. Atlam, Mater. Corros. 60 (2009) 813–819.
[29] W. Li, X. Zhao, F. Liu, J. Deng, B. Hou, Mater. Corros. 60 (2009) 287–293.
[30] R. Hasanov, M. Sadikoglu, S. Bilgic, Appl. Surf. Sci. 253 (2007) 3913–3921.
[31] M.A. Amin, K.F. Khaled, S.A. Fadl-Allah, Corros. Sci. 52 (2010) 140–151.
[32] M. Finsgar, A. Lesar, A. Kokalj, I. Milosev, Electrochim. Acta 53 (2008) 8287–8929.
[33] R.G. Pearson, Inorg. Chem. 27 (1988) 734–740.
[34] R.G. Pearson, J. Am. Chem. Soc. 85 (1963) 3533–3539.
[35] K.F. Khaled, M.A. Amin, Corros. Sci. 51 (2009) 1964–1975.
[36] K. Babic-Samardzija, C. Lupu, N. Hackerman, A.R. Barron, J. Mater. Chem. 15 (2005) 1908–1916.
[37] P. Zhao, Q. Liang, Y. Li, Appl. Surf. Sci. 252 (2005) 1596–1607.
[38] H.L. Wang, H.B. Fan, J.S. Zheng, Mater. Chem. Phys. 77 (2003) 655–661.
[39] S. John, A. Joseph, RSC Adv. 2 (2012) 9944–9951.

Please cite this article in press as: S. John et al., Corrosion inhibition properties of 1,2,4-Hetrocyclic Systems: Electrochemical, theoretical and Monte Carlo simulation studies, Egypt. J. Petrol. (2016), http://dx.doi.org/10.1016/j.ejpe.2016.10.005